LAWRENCE
LIVERMORE
NATIONAL
LABORATORY

UCRL-CONF-233678

Electrostatic Modeling of Vacuum Insulator Triple Junctions

L. K. Tully, A. D. White, D. A. Goerz, J. B. Javedani, T. L. Houck

August 14, 2007

IEEE Pulsed Power and Plasma Science Conference
Albuquerque, NM, United States
June 17, 2007 through June 22, 2007

ELECTROSTATIC MODELING OF VACUUM INSULATOR TRIPLE JUNCTIONS *

L.K. Tully, A.D. White, D.A. Goerz, J.B. Javedani, T.L. Houck
Lawrence Livermore National Laboratory, 7000 East Avenue
Livermore, CA, USA

Abstract

Triple junctions are often initiation points for insulator flashover in pulsed power devices. Two-dimensional finite-element TriComp and Maxwell modeling software suites were utilized for their electrostatic field modeling packages to investigate electric field behavior in the anode and cathode triple junctions of a high voltage vacuum-insulator interface [1,2]. Both codes enable extraction of values from a macroscopic solution for use as boundary conditions in a subset solution. Electric fields computed with this zoom capability correlate with theoretical analysis of the anode and cathode triple junctions within submicron distances for nominal electrode spacing of 1.0 cm. This paper will discuss the iterative zoom process with TriComp and Maxwell finite-element electric field solvers and review theoretical verification of the results.

I. INTRODUCTION

Vacuum insulators are critical components in high energy pulsed power devices. The triple junction of vacuum, dielectric, and metal creates a unique environment for field enhancement and attendant possibility for breakdown or flashover. Accurate field modeling of triple junctions facilitates insulator design with higher voltage standoff capabilities.

For efficient use of computer memory, the mesh generators in many commercial finite-element modeling codes employ adaptive mesh refinement, whereby the problem is solved on successively finer meshes. During each iteration, the algorithm selects regions with high perceived error and refines the mesh in those areas while leaving the mesh in areas with low perceived error relatively unaltered. The mesh generator in Ansoft Maxwell 2D uses this approach. In contrast, the Field Precision TriComp mesh generator (Mesh 5.0) builds a conformal mesh based on the user's mesh specifications. Mesh grid size can be adjusted in the x-y (or r-z) direction. A comparison between these two approaches is shown in Fig. 1.

Both codes permit a method of "iterative zooming" by assigning interpolated potential values from a closed path within the solution area as the boundary conditions for a new problem consisting of the enclosed area. This approach can be used to include small details after a global solution has been established. The zooming procedure may also be utilized to study areas of interest such as the anode and cathode triple junctions in extreme detail.

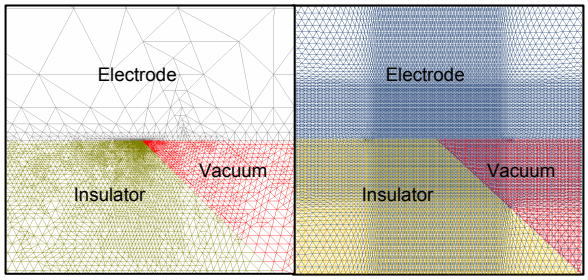

Figure 1. The mesh on the left was produced with Maxwell 2D and is the result of adaptive mesh refinement. The mesh on the right was constructed by TriComp Mesh 5.0.

II. MODEL

The two-dimensional modeled geometry consists of a disk-shaped anode and cathode with a truncated 45° cone insulator as shown in Fig. 2. The insulator is 1 cm in height and is positioned between the anode and cathode. This entire configuration is placed inside a vacuum chamber with walls at ground potential. The anode is charged to positive 100 kV while the cathode remains at ground potential.

Although the geometry of the device is rotationally symmetric about the r = 0 axis, the zooming procedure required the use of x-y coordinates with shift invariance in the z direction. The use of rectangular coordinates for this application is acceptable since the region of interest around the triple junction (submicron range) is significantly smaller than the curvature of the insulator itself.

* This work was performed under the auspices of the U.S. Department of Energy by University of California, Lawrence Livermore National Laboratory under Contract W-7405-Eng-48.

In the initial global geometry, as shown in Fig. 2, the anode and cathode were assigned fixed potential Dirichlet boundaries of 100 kV and 0 kV respectively. The 45° insulator region was assigned a dielectric constant of 2.8. The initial mesh in Tricomp was constructed with a 30 µm mesh in the regions of interest including the anode, cathode, and insulator. The outermost areas were constructed with a 50 µm mesh. In Maxwell 2D, the mesh was generated using adaptive mesh refinement and the problem was solved to convergence.

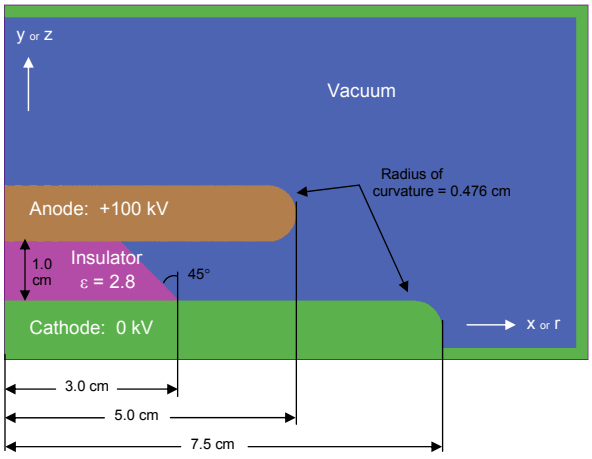

Figure 2. Global geometry: 6.0 cm x 10.0 cm

The potential lines and electric field magnitude of the entire region are seen in Fig. 3 and Fig. 4. Potential values along the boundaries were extracted (and interpolated) from calculated values along those same lines in the previous solution. In Tricomp, this process was automated by the code with user specified "zoom" levels. For the above described geometry, mesh sizes of 10, 5, 1, and 0.2 µm were constructed as the solution region was significantly reduced at each step. Using Maxwell 2D, the process must be done manually. The user must export and import the interpolated potential values from the boundaries of a closed region within the solution via ASCII files. This process was repeated four times for the described geometry to provide adequate resolution at the ATJ and CTJ.

Additionally, new features such as rounded tips or small cracks may be added with the use of old boundaries as long as the added features are located a reasonable distance away from the boundaries themselves [3]. This was not necessary in the baseline case investigation of the ATJ and CTJ, but it proves valuable during studies of imperfections in the triple junctions.

Line scans were taken from the solution on both the vacuum and insulator sides of the interface as seen in Fig. 5. In TriComp, the lines were one mesh size away from the insulator-vacuum interface and electrode surface. In Maxwell 2D, lines closer to the interface were taken due to the increasingly smaller mesh sizes along boundaries. The results from these line scans are plotted in Fig. 6. As expected, the tangential component of the electric field is the same on both the insulator and vacuum sides of the interface. The normal fields differ by a factor of the dielectric constant.

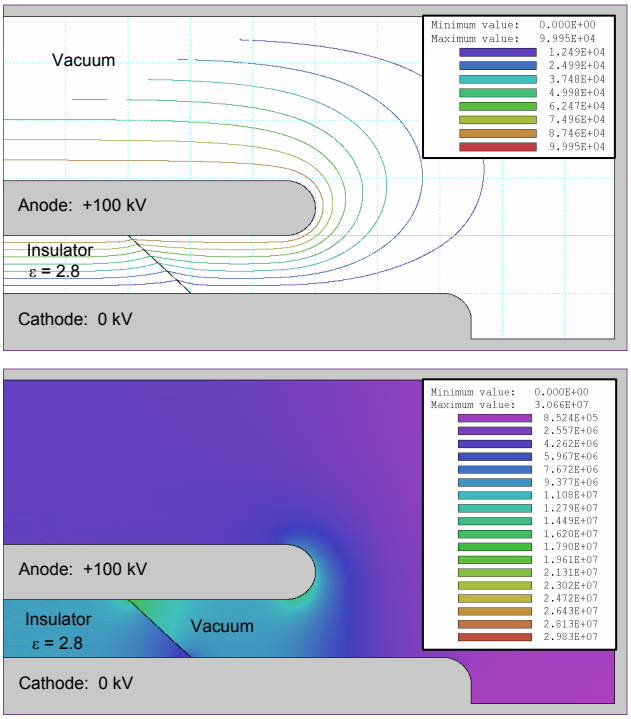

Figure 3. Potential and electric field results in TriComp global (initial) solution

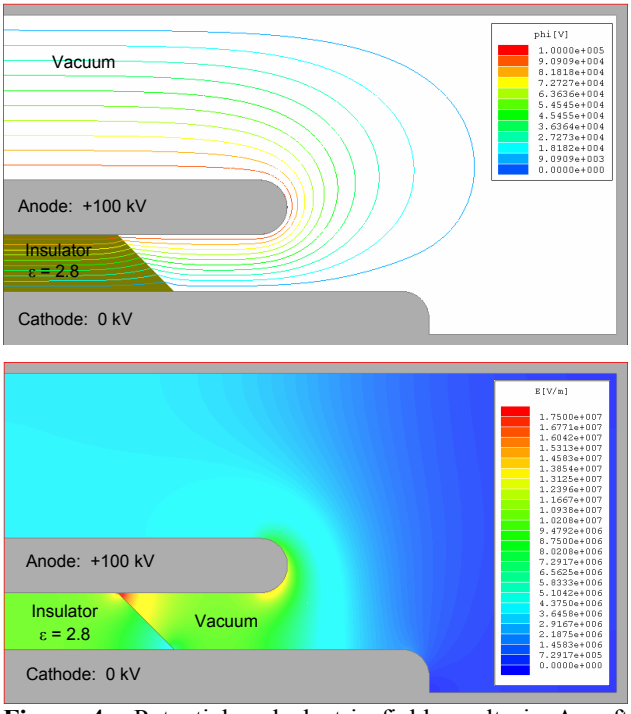

Figure 4. Potential and electric field results in Ansoft global (initial) solution

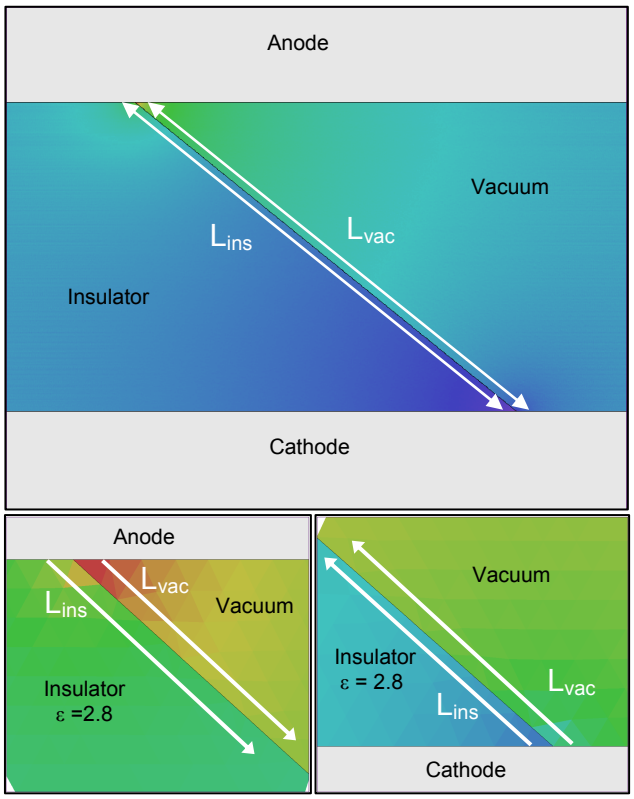

Figure 5. Definition of line scans taken along vacuum-insulator interface (10 and .2 μm TriComp meshes shown)

The maximum and minimum values in Table 1 are taken approximately one mesh size away from the triple junction in the TriComp solution. With each mesh size decrease (or zoom increase) it can be noted that the electric fields increase at the ATJ and decrease at the CTJ. It can be shown theoretically through the work of Takuma and Chung that the classical theoretical value of the electric field approaches infinity at the anode triple junction and approaches zero at the cathode triple junction [4-8]. A summary of their approaches is given in the next section.

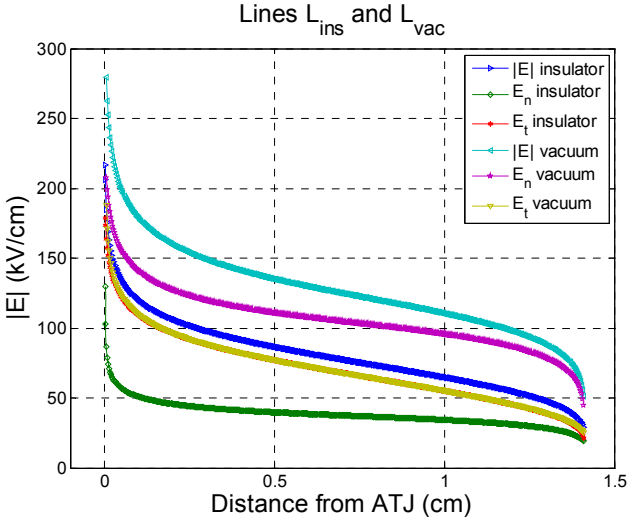

Figure 6. Line scan from ATJ to CTJ

Table 1. Increasing/decreasing electric field strength at ATJ/CTJ with decrease in TriComp mesh size

Mesh size (μm)	Max |E| field at ATJ (kV/cm)	Min |E| field at CTJ (kV/cm)
30	302	47
10	331	39
5	391	35
1	499	27
0.2	638	21

III. THEORY

Chung et al. describes the electric field strength in the vacuum near a 2D triple junction for small r (radial distance from the triple junction) as

$$E = Cr^{\nu-1} \tag{1}$$

where C and ν are constants [6-8]. The transcendental equation

$$\varepsilon \tan(\nu\theta) = \tan(\pi - \nu\beta) \tag{2}$$

defines ν based upon the angles described in Fig. 7 and the dielectric constant ε.

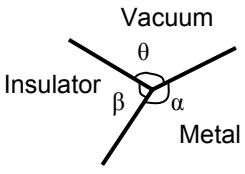

	ATJ	CTJ
Metal (α)	π	π
Insulator (β)	3π/4	π/4
Vacuum (θ)	π/4	3π/4

Figure 7. Definition of angles by Chung et al. and the corresponding values for the modeled geometry

Therefore, for the modeled 45° insulator case, the value of ν at the ATJ is 0.84778 and ν at the CTJ is 1.15222. From Eq. (1), the electric field strength at the ATJ and CTJ are written as

$$E_{ATJ} = Cr^{-0.15222} \tag{3}$$

$$E_{CTJ} = Cr^{+0.15222} \tag{4}$$

As $r \to 0$,

$$E_{ATJ} \to \infty \tag{5}$$

$$E_{CTJ} \to 0 \tag{6}$$

In the dielectric, the electric field strength also approaches infinity at the ATJ and zero at the CTJ.

Electric field strength in the dielectric in relation to the field strength in the vacuum can be expressed

$$E_{ins} = \eta E_{vac} \tag{7}$$

where

$$\eta = \frac{\sin(\nu\theta)}{\sin(\nu\beta)}. \tag{8}$$

For the modeled 45° insulator case, η at the ATJ is 0.67858 and η at the CTJ is 0.52633.

Given this set of theoretical benchmarks, comparisons between the computed values and the modeled case were drawn. The accuracy of the "zooming" method and its use as an analysis tool for small details in a large solution space was also studied.

IV. ANALYSIS

The theory noted in the previous section provides excellent groundwork for triple junction electrostatic model verification. The model described in Sec. II was evaluated at all stages of the zooming process. Model output included electric field values and the corresponding coordinates. The most information about the validity of zooming procedure was gleaned from the final mesh. The initial mesh (global case) provided a useful demonstration of the assumptions or limitations used in the analytical model.

From the initial line scans described in Sec. II and shown in Fig. 5 and Fig. 6, it can be concluded that the shape of the curves is concurrent with Eq. (5) and Eq. (6). Assuming that the curves also agreed with Eq. (1), the analysis of the model began with the calculation of ν. Stating Eq. (1) in a different form,

$$\ln(E) = (\nu - 1)\ln(r) + \ln(C) \tag{9}$$

The linearity of the plots in Fig. 8 through Fig. 11 can be exploited to determine ν values for both the ATJ and CTJ. The slopes of the ATJ line scan data in Fig. 8 and Fig. 9 in the insulator and vacuum are remarkably similar to the theoretical value of -0.15222 stated in the previous section. The same holds true for the CTJ theoretical value of 0.15222. Corresponding ν values are noted on the plots.

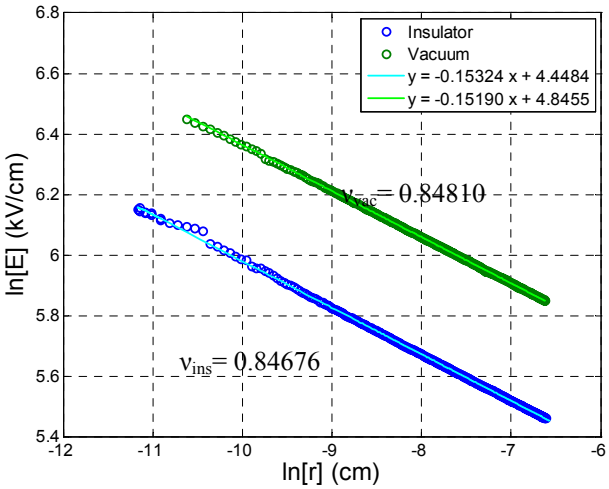

Figure 8. ATJ line scan data from final TriComp mesh

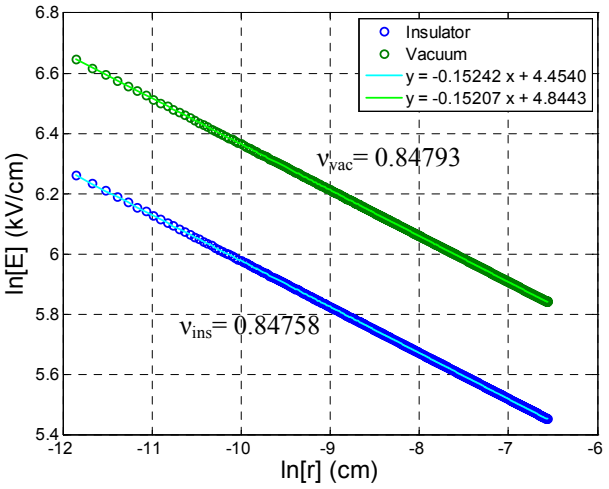

Figure 9. ATJ line scan data from final Ansoft mesh

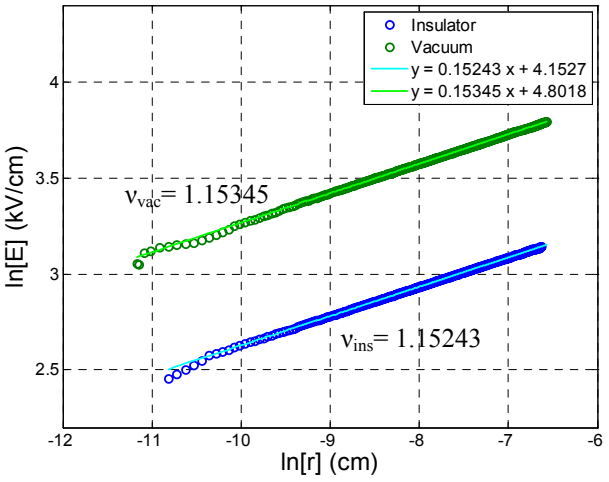

Figure 10. CTJ line scan data from final TriComp mesh

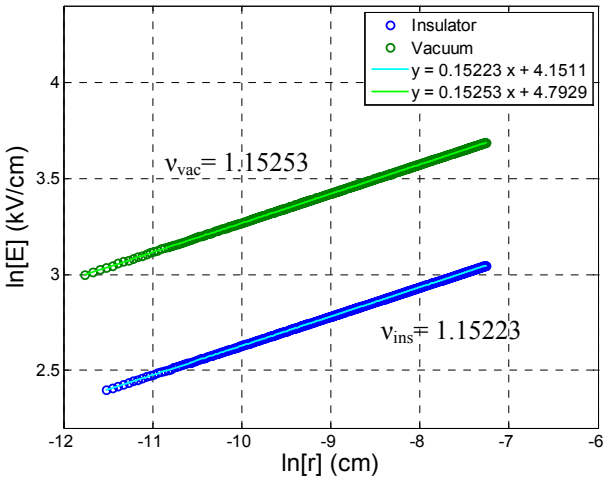

Figure 11. CTJ line scan data from final Ansoft mesh

Another comparison may be drawn from the relationship between line scan values in the vacuum and the insulator. Eq. (7) and Eq. (8) describe the relationship between the electric field strength in vacuum and insulator. Considering the theoretical η values from the previous section and the final zoom data, less than 0.5% difference is seen in either model until a distance of approximately 1 micron from the ATJ or CTJ. The results are seen in Fig. 12 and Fig. 13.

Compared to Maxwell 2D, the TriComp model η percent difference increases at a distance further away from the triple junctions. This is due to the nature of the mesh construction. Near the triple junctions, the field strength is changing rapidly and the TriComp mesh size remains static. The Maxwell 2D adaptive mesh reduces in size near the junctions and more closely represents the field in the area. Although, the application of the iterative zoom technique does not necessitate fine resolution of the field except at the boundary locations used for the following zoom.

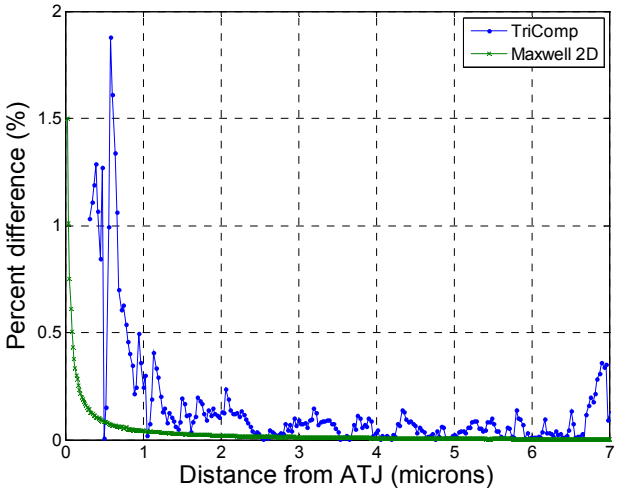

Figure 12. Percent difference between modeled and theoretical η nearing ATJ

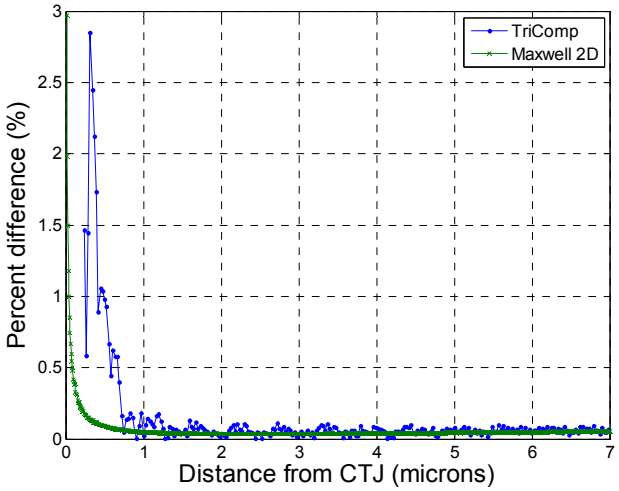

Figure 13. Percent difference between modeled and theoretical η nearing CTJ

A final theoretical and computational comparison can be made from Eq. (1) [9]. The values of r and ν are known or can be computed from the geometry. Electrostatic field modeling allows for the calculation of C. Combining the theoretically calculated ν value and computationally calculated C value, a plot can be constructed to show the relationship between the fields obtained from software and the fields near the triple junctions obtained from a combination of software (C) and theory (ν). The relationship is plotted in Fig. 14.

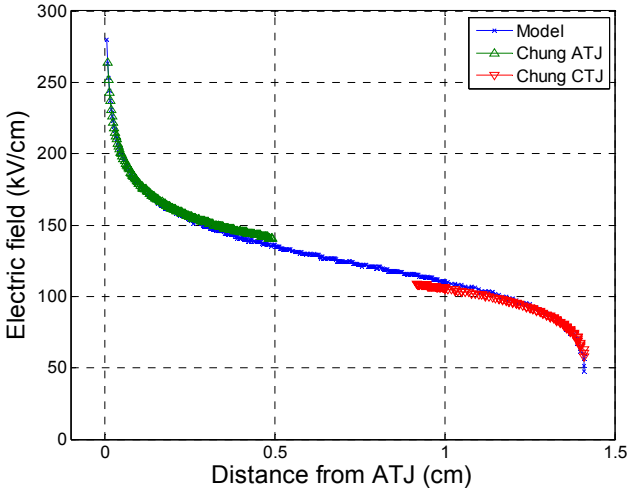

Figure 14. Relationship of computed fields to theoretical fields

V. SUMMARY

A baseline 45° degree insulator case was modeled using the electrostatic solvers of both TriComp and Maxwell 2D. An iterative "zoom" procedure was employed to study the anode and cathode triple junctions

at a submicron level. Results from such models were compared to the analytical analysis provided by Chung et al. Good correlation between the analytical and computational methods was noted. In these studies, the iterative zooming achieved with both codes appears to be a powerful modeling technique.

VI. REFERENCES

[1] Field Precision LLC, PO Box 13595, Albuquerque, NM 87192. www.fieldp.com

[2] Ansoft Corporation, 225 West Station Square Drive, Suite 200, Pittsburgh, PA 15219. www.ansoft.com

[3] TriComp 5.0, EStat: Finite-element Electrostatics, Field Precision, 2002.

[4] T. Takuma, T. Kouno, and H. Matsuda, "Field behavior in composite dielectric arrangement", *IEEE Trans. Electr. Insul.*, vol. EI-13, no 6, pp. 426-435, Dec. 1978.

[5] T. Takuma, "Field behavior at a triple junction in composite dielectric arrangements", *IEEE Trans. Electr. Insul.*, vol. 26, no. 3, pp. 500-509, June 1991.

[6] M.S. Chung, B-G. Yoon, P.H. Cutler, and N.M. Miskovaky, "Theoretical analysis of the enhanced electric field at the triple junction", *J. Vac. Sci. Technol. B*, vol. 22, no. 3, pp. 1240-1243, May 2004.

[7] M.S. Chung, T.S. Choi, B-G. Yoon, "Theoretical analysis of the field enhancement in a two-dimensional triple junction", *Applied Surface Science*, vol. 251, no. 1-4, pp. 177-181, Sept. 2005.

[8] M.S. Chung, S.C. Hong, P.H. Cutler, N.M. Miskovsky, B. L. Weiss, A. Mayer, "Theoretical analysis of triple junction field emission for a type of cold cathode", *J. Vac. Sci. Technol. B*, vol. 24, no. 2, pp. 909-912, Mar. 2006.

[9] W.A. Stygar, J.A. Lott, T.C. Wagoner, V. Anaya, H.C. Harjes, H.C. Ives, Z.R. Wallace, G.R. Mowrer, R.W. Shoup, J.P. Corley, R.A. Anderson, G.E. Vogtlin, M.E. Savage, J.M. Elizondo, B.S. Stoltzfus, D.M. Andercyk, D.L. Fehl, T.F. Jaramillo, D.L. Johnson, D.H. McDaniel, D.A. Muirhead, J.M. Radman, J.J. Ramirez, R.B. Spielman, K.W. Struve, D.E. Walsh, E.D. Walsh, and M.D. Walsh, "Improved design of a high-voltage vacuum-insulator interface", *Phys. Rev. ST Accel. Beams 8*, 050401, May 2005.